Single, simultaneous and consecutive biosorption of Cr(VI) and Orange II onto chemically modified masau stones

Albadarin, A. B., Solomon, S., Mangwandi, C., & Kurniawan, T. A. (2017). Single, simultaneous and consecutive biosorption of Cr(VI) and Orange II onto chemically modified masau stones. Journal of Environmental Management, 204(1), 365-374. https://doi.org/10.1016/j.jenvman.2017.08.042

Published in:
Journal of Environmental Management

Document Version:
Peer reviewed version

Queen's University Belfast - Research Portal:
Link to publication record in Queen's University Belfast Research Portal

Single, Simultaneous and Consecutive Biosorption of Anionic Cr(VI) and Orange II onto Chemically Modified Masau Stones

Ahmad B. Albadarin[1,2*], *Samuel Solomon*[1], *Tonni Agustiono Kurniawan*[3], *Chirangano Mangwandi*[2], *Gavin Walker*[1]

[1]*School of Natural Sciences, Bernal Institute – University of Limerick – Limerick, Ireland.*

[2]*School of Chemistry and Chemical Engineering – Queen's University Belfast – Belfast BT9 5AG, Northern Ireland UK.*

[3]*College of Ecology & Environment, Xiamen University, Xiamen 361102, Fujian Province, China*

**Corresponding author: E-mail: Ahmad.B.Albadarin@ul.ie. Tel: +353-(0)-61-237732.*

ABSTRACT

Novel and low cost chemically modified masau stone (CMMS) was investigated for its biosorption of an anionic azo dye, Orange II (OII), and toxic hexavalent chromium (Cr(VI)) from aqueous systems: individually, simultaneously and consecutively. The effects of pH, contact time and initial concentration (C_o), and loading order on mechanisms of biosorption/reduction of OII and Cr(VI) onto CMMS were examined in detail. Several analytical techniques were employed to characterise the physio-chemical properties of the CMMS and determine the biosorption mechanisms. The pseudo second order and redox models were able to adequately predict the kinetics of biosorption.

The Langmuir maximum OII biosorption capacity (q_{max}) was calculated as 136.8mg/g for the dye onto the Cr(VI)-loaded CMMS consecutive system at C_o = 100mg/dm^3. The q_{max} for the Cr(VI) system was found to be 87.32mg/g at the same C_o max. XPS and FTIR analyses indicated the introduction of quaternary-Nitrogen to the CMMS surface after activation and the involvement of carboxyl, sulphonate and hydroxyl groups in OII and Cr binding mechanisms. It was confirmed that the biosorption of OII and Cr(VI) mainly takes place via two different mechanisms i.e. hydrogen bonding and electrostatic attraction for the dye, and biosorption-coupled reduction for Cr(VI).

Keyword: Orange II; Hexavalent Chromium; Binary; Consecutive Biosorption; Bioremediation.

1. INTRODUCTION

Dyes and metals are pollutants found in wastewaters (Albadarin and Mangwandi, 2015; Albadarin et al., 2014b). These types of environmental pollutants are often toxic, carcinogenic,

and pose serious problems, even in minute concentrations (Ferhat et al., 2016). More than 8000 chemical products are associated with the dyeing process with 2% of the annually produced dyes (Almost 10^9 kg, 70% of which are azo dyes) discharged directly in aqueous effluents (Fanun, 2014; Liu et al., 2016; Salvi and Chattopadhyay, 2016). Amongst these azo dyes, Orange II (OII) is one of the most widely used reactive dyes in the textile dyeing industries (Heibati et al., 2015).

Toxic metals such as chromium (Cr), lead (Pb), arsenic (As), and mercury (Hg) are increasingly used in many areas for day-to-day activities (Naushad et al., 2016; Salameh et al., 2015). Hexavalent chromium, Cr(VI), oxyanions are found as contaminants in water, and when compared to other toxic metals, Cr(VI) is relatively soluble in the aqueous phase over nearly the entire pH range (Babel and Kurniawan, 2004; Li et al., 2017). Moreover, Cr(VI)–dyes complexes used for dye fixation in wool dyeing are problematic compounds of wastewaters with the levels of Cr(VI) in wool dying wastewaters detected in the range of 1–13 mg/dm^3 (Correia et al., 1994).

Several studies have investigated the use of various physicochemical and biological treatment methods of Cr(VI) and dyes, individually and simultaneously based on practicality and industrial value (Anandkumar and Mandal, 2011; Kyzas et al., 2013; Li et al., 2016). Treatment techniques include: ion exchange, chemical precipitation and electrodialysis which in many cases present significant disadvantages such as high energy intensity, high reagent consumption, etc. Adsorption and biosorption processes, on the other hand, present a low cost and highly effective alternative in the removal of dyes and heavy metals from aqueous solutions (Gómez et al., 2014; Kurniawan et al., 2006). As a result, much effort has been invested in the research of low cost and efficient adsorbents, including the use of novel materials such as modified zeolites (Song et al., 2015) and cerium immobilized cross-linked chitosan composites (Zhu et al., 2017).

However the use of raw biomaterials, both natural and by-product, for this purpose have been shown to provide comparable adsorption capacities (Daneshvar et al., 2013; Karthik et al., 2017; Mishra et al., 2016; Šillerová et al., 2014; Wu et al., 2011). Previous studies have proven

that aminated biomasses are very efficient when employed for the removal of anionic dyes and Cr(VI) oxyanions (Cao et al., 2014; Deng and Ting, 2005).

Therefore, this study was dedicated to: (i) use the chemically modified masau stone (CMMS), for the first time, to remove Orange II (OII) and Cr(VI) from single aqueous solution; (ii) compare the results from (i) in removing the two anions from multi-component systems and consecutive biosorption (iii) use various analytical techniques such as XPS, FTIR and SEM to comprehensively investigate the biosorption mechanisms and determine if OII and Cr(VI) compete for the biosorption sites or can be removed simultaneously or one after another.

2. EXPERIMENTAL METHODS

2.1. Preparation of chemically modified masau stone, CMMS

Masau stone (MS) biomass, (Ziziphus mauritiana), was collected and crushed (350–500µm), repeatedly washed with distilled water and dried at 90ºC until constant weight. The chemical modification procedure of MS was carried out as follows: (i) 4g of the cleaned MS was mixed with a solution containing 60 cm^3 of 1.5M NaOH and 40 cm^3 epichlorohydrin on a hotplate at 40°C for 45min; (ii) the MS was then filtered and washed several times with deionized water and dried; (iii) after that, the MS obtained from (ii) was mixed with 60 cm^3 of 1.5M NaOH and 10 cm^3 of diethylenetriamine (DETA) and the mixtures was stirred at 60°C for 90min; (iv) finally, the CMMS was filtered, washed with deionized water and dried in an oven at 90°C overnight.

2.2. Hexavalent chromium (Cr(VI)) and Orange II (OII)

Potassium dichromate ($K_2Cr_2O_7$) and Orange II sodium salt ($C_{16}H_{11}N_2NaO_4S$) from Sigma–Aldrich (UK) were used to prepare stock solutions and subsequently diluted with deionized water to required concentrations. Hexavalent chromium, Cr(VI), concentrations were determined using a standard method (Albadarin et al., 2011a) using UV/Vis Perkin Elmer LAMBDA 25, UK spectrophotometer at λ = 540nm. Total chromium concentrations were analysed by an inductively coupled plasma (ICP-AES Perkin-Elmer 400 series) at wavelength

285nm. The trivalent chromium concentrations were calculated as: Cr(III) = CrTotal – Cr(VI) and the OII dye concentrations were determined by UV/Vis spectrophotometer at λ = 478nm (The UV–vis absorption spectra of this dye at different pH were identical).

2.3. Biosorption experiments

Solution pH effects (pH range 2 – 8) were investigated (volume = 25cm^3; C_o = 100mg/dm^3 and temperature = 20ºC) by adding CMMS to glass jars containing the solutions (Dose = 2g/dm^3) and measuring the equilibrium concentrations of Cr(VI) and OII at 1 pH unit increments. Samples were shaken for 24hrs on a mechanical shaker and filtered through a 0.45µm membrane filter to remove the CMMS. The optimal pH samples were used for surface characterisations after the biosorption processes.

Kinetic experiments with a solution volume of 250cm^3 were performed on hotplate stirrers for 6hr using the same parameters and conditions. The Cr(VI)-loaded CMMS and OII-loaded CMMS were collected, washed with deionized water and dried. As the adsorbates were chemically bonded onto the adsorbent it was assumed that no leaching occurred, which was further confirmed by SEM and XPS results. Consecutive biosorption was investigated by using the Cr(VI)-loaded CMMS and OII-loaded CMMS for biosorption of OII and Cr(VI), respectively. The isotherm studies for the metal and dye single solutions, multi-component and consecutive solutions were carried out at C_o = 50mg/dm^3 – 300mg/dm^3 and 20ºC and the solutions were continuously shaken for 24h. All experiments in this section were carried out in duplicate with negligible error margin. The metal and dye loading, q (mg/g), and percentage of removal (%) were calculated using Eq. (1) and (2), respectively:

$$q = \left[\frac{C_o - C_e}{M}\right] \times V \qquad (1)$$

$$\text{The percentage removal} = \left[1 - \frac{C_e}{C_o}\right] \times 100\% \qquad (2)$$

where C_o is the initial and C_e is the equilibrium concentration of adsorbates in mg/dm^3, M is the amount of CMMS in g and V is the volume in dm^3.

2.4. Determination of surface characteristics and functional groups

The surface functional groups of the CMMS were determined by Fourier Transform Infrared (FTIR) Spectroscopy using a Perkin Elmer Spectrum 100 within the range of 4000–400/cm. The zeta potential measurements were carried out using a Malvern Zetasizer (3000HS). The specific surface area of maCMMS was measured by the N_2-BET method. For Scanning Electron Microscope (SEM) analysis, samples were coated with gold and vacuumed (5−10min) for electron reflection prior to analysis on a JEOL-JSM 6400 scanning microscope. The X-ray photoelectron spectroscopy (XPS) analysis was mainly employed to verify the oxidation state of the Cr bound to the CMMS surface. The Kratos ULTRA spectrometer was used for the XPS measurements with the following parameters: sample temperature = 20-30^{o}C; X-Ray Gun mono Al Kα 1486.58 eV; 150 W (10mA, 15kV) and pass Energy = 160eV for survey spectra and 20eV for narrow regions.

3. RESULTS AND DISCUSSIONS

3.1.Surface area, zeta potential and functional groups

The BET surface area of the unloaded chemically modified masau, CMMS, was measured as 77.32m^2/g. The total pore volume and average pore radius CMMS are 0.081cm^3/g and 21.32Å, respectively. After Cr(VI) biosorption induced reduction, the surface area of the Cr(III) loaded CMMS increased to 132.35m^2/g. The zeta potential profile of CMMS showed a strong pH-dependence with the CMMS adsorbent exhibiting positive zeta potential values at pHs lower than 3.8 (Figure 1A), which may be due to the formation of positive CMMS–NH_3^+ sites at lower pH values. A pH above this value initiates deprotonation, resulting in a decrease in biosorption capacities of the CMMS adsorbent, especially for anionic species (Albadarin et al., 2011b). The FTIR analysis for the raw and chemically activated MS is shown in Figure 1B. The broad band located at 3358–3377/cm for the MS in Figure 1B can be assigned to –OH, –SiOH and –NH stretching vibrations of hydroxyl groups. The peak around 2900/cm is attributed to alkyl –C–H stretching.

Peaks around 1422/cm are due to –C–H bending and asymmetric $–SO_3$ bands can be detected around 1329/cm (Deng et al., 2003). After chemical activation, peaks around 2100/cm, 1600/cm and 1100/cm are assigned to –C≡N, –NHCO and –C–N stretching, respectively. This demonstrates that the chemical modification has embedded many amine groups onto the CMMS surface. Also, a stronger broad band around 3100 to 3700/cm indicates that several –OH and –NH groups were formed on the surface of the CMMS. The new hydroxyl and amine groups will contribute to the removal of Cr(VI) and OII and increase the biosorption capacity via the formation of columbic forces, hydrogen bonds and π– π interactions. The quantitative XPS analysis from the high resolution spectrum indicated that the concentration of nitrogen atoms nearly doubled after MS modification. This confirmed that more –NH groups were introduced to the surface of the CMMS. More details are provided in section 3.6.2.

3.2. Effect of solution pH

The biosorption of Orange II (OII) and Cr(VI) in single and multi-component systems as functions of solution pH are shown Figure 1. It was found that for single systems, above 90% of OII dye and 80% Cr(VI) removal occurred at pH = 2 and 3. For the Orange II dye, the lowest removal was observed at pH 8, approximately 60%, which is considered a very good removal percentage bearing in mind the C_o of the dye and amount of CMMS used.

The pH dependence of Cr(VI) and OII simultaneous uptakes were rather comparable to those in their corresponding single pollutant systems as revealed in Figure 1. For the multi-component system, the CMMS was still able to remove substantial amounts of Cr(VI) and OII at pH 2, and 4. This indicated that the anionic species of Cr(VI) and dye did not compete for the biosorption sites when co-existing in the same solution and instead, OII biosorption improved over the pH range studied. Similar observations were reported for the adsorption of OII and Cr(VI) using quaternary ammonium salt modified chitosan magnetic composite adsorbents (Li et al., 2016). However, it is worth mentioning that the possibility of Cr(VI) reduction by the modified chitosan was not considered in this previous study.

158 The CMMS can attract the OII dye molecules by both electrostatic attraction and through
159 the formation of surface hydrogen bonds/π– π interactions between the amine and hydroxyl
160 groups on the CMMS surface and the nitrogen and oxygen atoms of OII dye. The good OII
161 biosorption over the entire pH range could be attributed to the interaction between the CMMS
162 surface and π-electron system of the dye. The more noticeable decrease in the biosorption
163 efficiency for Cr(VI) is typically common when using bio-based-materials where the biosorption
164 mechanism is described by the biosorption-reduction model (Albadarin et al., 2014a). At low
165 pH, Cr(VI) anions can oxidize secondary alcohol groups while being reduced to Cr(III) cations.
166 After biosorption, both Cr(VI) and Cr(III) species were found in the aqueous solution with
167 approximately 10% of the Cr(VI) that initially existing converted to Cr(III). At pH > 4,
168 dissociation of functionalities such as –COOH, $–SO_3$ and –SiOH leads to increased negative
169 charge on the CMMS, thus, anionic Cr(VI) species might be repelled at these pHs. At pH = 7
170 where the minimum amount of Cr(VI) was removed (42.3% removal), only 2% of the reduced
171 Cr(VI) was detectable in the aqueous solution. The bound Cr(III) species can also form surface
172 complexes with the protonated functional groups, such as $–NH_2$, –COOH and very active –SiOH
173 groups on the CMMS surface. The removal of Cr(VI) decreased by about 10% in the multi-
174 component system; the equilibrium Cr(III) concentration was less than 5% of the Cr(VI) initial
175 concentration. This is attributed to the existence of Cr(III) in the solid phase, acting as a ligand
176 between the dye molecules and the CMMS adsorbent, and additionally reducing the repulsion
177 forces between the dye molecules.
178 Also, after Cr(VI) was biosorbed and reduced to Cr(III) to the CMMS, the surface area of
179 the CMMS increased as indicated by the BET results. Similar observations were published for
180 Cr(III)-loaded adsorbents used for further anionic dyes biosorption (Bouberka et al., 2006), in
181 which the BET surface area increased from 110 to 317m^2/g after Cr(III) loading. This
182 demonstrates that there is an ample number of active sites which the Cr(VI) and OII molecules
183 can bind to i.e. unoccupied sites as well as to the Cr(III)-intercalated sites. However, in order to

avoid the precipitation of OII dye, all following experiments were carried out at approximately pH = 3.5.

3.3. Contact time: single, simultaneous and consecutive biosorption

The contact time experiments were performed using fresh CMMS for single and multi-component systems and Cr(VI)-loaded-CMS and OII-loaded-CMMS for OII and Cr(VI) consecutive biosorption at pH = 3.5, respectively, and the results are revealed in Figure 2. Results indicate that the biosorption phenomena occurs over a short time period. The plots show that the kinetics of biosorption primarily consist of two periods: an initial rapid period associated with the instant external surface biosorption of metal ions/molecules. The fast removal of OII and Cr(VI) is perhaps due to the electrostatic attraction, extracellular bio-reduction, micro-precipitation and cellular affinity (Mungasavalli et al., 2007; Volesky, 2007).

The second slower period was the gradual biosorption stage that occurred before metal ions and dye molecules uptake reached equilibrium. The time required for OII and Cr(VI) to reach equilibrium was very similar, however, the initial rate of reaction for OII seemed faster but gradually decreased due to the limited number of biosorption sites at the fixed concentrations. A related increase in the Cr(III) concentration (5 to 10% of C_o of Cr(VI)) in the aqueous solution was observed as the Cr(VI) decreased with time, (Figure 2). The slower Cr(VI) removal was attributed to the fact that Cr(VI) was first biosorbed onto CMMS and then reduced to Cr(III) (Albadarin et al., 2013). Cr(III) was not initially present in the solution and this confirmed that Cr(VI) was reduced to Cr(III) when in contact with the CMMS surface.

When Cr(VI) and OII co-existed in the same solution, the simultaneous biosorption of OII dye was very fast and efficient. This suggested that the energetically less favourable sites become available for biosorption with an increase in the ions/molecules concentration. As for Cr(VI), the removal percentage decreased but the amount of desorbed Cr(III) as a result of repulsion with the positively charged functional groups on the CMMS surface decreased. These results were in good agreement with the pH results.

In order to confirm these phenomena, the loaded-CMMS materials were used for Cr(VI) and OII consecutive biosorption at pH = 3.5 and C_o = 100mg/dm^3. Interestingly, the cross-matched loaded-CMMS materials could efficiently biosorb OII and biosorb-reduce Cr(VI) with very similar percentage removals to those obtained from the multi-component systems. This confirmed that the biosorptions of OII and Cr(VI) were taking place by two different mechanisms i.e. hydrogen bonding/π– π interactions and electrostatic attraction for the dye, and biosorption coupled reduction for Cr(VI).

3.4. Kinetic modelling

The pseudo first and second order (Ho and McKay, 1999; Lagergren, 1898) and intra-particle diffusion models were used to describe the kinetic data tested:

$$q_t = q_e\left(1 - e^{-k_1 t}\right) \quad (3)$$

$$q_t = \frac{k_2 q_e^2}{\left(1 + k_2 q_e t\right)} t \quad (4)$$

where k_1 (1/min) is the pseudo first order, k_2 (g/mg min) is the pseudo second order rate constants.

It has been proven that the Cr(VI) reactions which take place on the activated and raw biomass surfaces do not follow simple reaction order kinetics due to the finite number of surface sites available for the reaction to occur. So, the kinetics of Cr(VI) biosorption-reduction onto CMMS was modelled using the redox model, as follows (Park et al., 2007):

$$[\mathrm{Cr(VI)}] = \frac{C_{OC}[B][\mathrm{Cr(VI)}]_o - [\mathrm{Cr(VI)}]_o^2}{C_{OC}[B]\exp(k_{redox}(C_{OC}[B] - [\mathrm{Cr(VI)}]_o)t) - [\mathrm{Cr(VI)}]_o} \quad (5)$$

where k_{redox} is the rate coefficient, B is the biomass and C_{OC} indicates the content of the equivalent organic compound per unit gram of biomass, mg/g.

The fittings for the pseudo first and second order models and their calculated constants are shown in Figure 2 and Table 1. It can be concluded that, to a certain extent, both models were able to represent the kinetic data ($R^2 \geq 0.980$). This is also in agreement with previous

studies (Albadarin et al., 2012; Albadarin et al., 2014b). The fact that these models are empirical equations and do not give a precise explanation of the chemical and physical processes, should be considered. However, in the case of Cr(VI) biosorption onto fresh CMMS and OII biosorption onto Cr(VI)-loaded CMMS, the second-order-model was able to describe the biosorption process with higher accuracy (R^2 value close to unity and low difference between calculated q_e and q_{exp}).

The k_1 and k_2 values for the OII biosorption onto CMMS are higher than that for the Cr(VI). These values decreased for Cr(VI) biosorption when co-existing with OII and declined further for the consecutive biosorption. On the other hand, k_1 and k_2 values increased for the OII biosorption onto CMMS. Larger k values suggest that for these systems, a shorter time is needed to reach a specific fractional uptake; as shown in Figure 3, the fractional uptake f vs time, t, where $f = q_t/q_e$. Also, the calculated values for the rate constant of external mass transfer, k_s, determined from the plots of C_t/C_o against time for all systems are given in Table 1 (plots are not shown here). The k_s increased for OII but decrease for Cr(VI) in multi-component and consecutive systems. This is attributed to the OII molecules having less competition for accessible surface area as the biosorption of Cr(III) increased the number of active sites. The reduction reaction of Cr(VI) to Cr(III) is very fast, the fact that the biosorption of OII dye is faster than that for Cr(VI), support the assumption that Cr(VI) was first electronically attracted to the positively charged groups before being reduced to Cr(III) by neighbouring electron-donor groups (Albadarin et al., 2013).

The redox model fitting for the biosorption of Cr(VI) onto fresh CMMS is also shown in Figure 2. The model was able to accurately predict Cr(VI) biosorption data, confirming that Cr(VI) was reduced when put in contact with CMMS. The model assumes that the rate equation of Cr(VI) reduction is a first order equation with respect to both Cr(VI) concentration and concentration of organic compound at constant pH and temperature. The redox reaction rate constant, k_{redox}, (Table 1) and content of organic compounds, C_{OC}, values decreased when Cr(VI)

co-existed with OII in the biosorption system. This could be due to the partial, however low, competition between the Cr(VI) ions and the dye molecules before Cr(VI) reduction to Cr(III).

Remarkably, according to Table 1, the values of redox model constants, k_{redox} and $C_{OC,}$ for CMMS are very similar to the second order model constants, k_2 and q_e (mg/g), values. This indicates that the second order model was able to predict the Cr(VI) biosorption mechanism (biosorption-reduction) and that the redox model accurately determined the organic compounds available for this reaction to take place. These models are useful in describing the removal mechanisms in spite of the lack of a complete understanding about the redox reaction between Cr(VI) and various unknown components on the CMMS surface.

3.5. Isotherm studies: single, simultaneous and consecutive biosorption

The biosorption data for Cr(VI) and OII was tested by Langmuir (Langmuir, 1916), Freundlich (Freundlich, 1906) and Redlich-Peterson (Redlich and Peterson, 1959) isotherm models:

Langmuir isotherm: $$q_e = q_{\max}\left[\frac{bC_e}{1+bC_e}\right] \quad (6)$$

Freundlich isotherm: $$q_e = K_F C_e^{1/n} \quad (7)$$

Redlich-Peterson isotherm: $$q_e = \frac{K_R C_e}{1+a_R C_e^{\beta}} \quad (8)$$

where q_{max} (mg/g) and b (dm^3/mg) are the Langmuir isotherm constants; K_F (mg/g (dm^3/mg)$^{1/n}$) is the biosorption capacity and $1/n$ is a measure of biosorption intensity; K_R (dm^3/g) and a_R are the Redlich-Peterson isotherm constants, where $0 \leq \beta \leq 1$.

The isotherm constants for the biosorption processes of OII and Cr(VI) onto CMMS at different systems are presented in Table 2 (Examples for the isotherm fittings are included in the supplementary data, SD1). Levels of Cr(III) detected in the Cr(VI) biosorption systems were less than 7% at all concentrations and, in this case, Cr(III) concentrations were not considered in the isotherm modelling. From Table 2, the Redlich-Peterson isotherm model was able to characterise the biosorption process in most cases with similar R^2 values to those for the Langmuir isotherm.

283 This suggests monolayer biosorption dynamic chemisorption processes by the biosorption
284 affinity in terms of surface functional groups and bonding energy where the biosorption
285 occurring at definite localized sites that are identical and equivalent. Also, this suggests that there
286 is no steric hindrance between that Cr(VI) and the OII molecules.

287 For the Cr(VI) biosorption onto CMMS, the process was also described well by the
288 Freundlich isotherm, and the β value for the Redlich-Peterson model was the smallest, indicating
289 that the process is not restricted to the formation of monolayer. The R^2 values for the Langmuir
290 and Redlich-Peterson isotherms were relatively low for the Cr(VI) binary biosorption system.
291 This behaviour could be explained as a change in the mechanism of the chromium biosorption
292 process. Chromium was initially biosorbed and reduced onto the first layer of the biosorbent
293 surface as Cr(VI) at low chromium concentration; however, when it reached its saturation,
294 another biosorption phenomenon (i.e. complexation) occurred by means of a chromium (Cr(VI)
295 and Cr(III)) biosorption process onto the multi-layer CMMS surface. The 1/*n* values for those
296 two systems were the lowest (closer to zero) showing that the CMMS surface is more
297 heterogeneous. K_F values increased for Cr(VI) and OII binary biosorption systems confirming
298 that the CMMS has a greater biosorption tendency towards the adsorbates in these systems. So,
299 it is obvious that Cr(VI) and OII are biosorbed differently.

300 *3.6. Proposed mechanisms*

301 3.6.1. XPS analysis

302 *3.6.1.1. Analysis for MS and CMMS before biosorption*

303 The surface analysis of raw MS and CMMS was performed using XPS. The survey scans
304 of these samples indicated the presence of carbon, oxygen, nitrogen, sulphur and silicon (Table
305 3). It seems that the major component among these N moieties was already present on the MS,
306 and as indicated, corresponded to the pyrrolic-N. The already existing amine groups on the
307 surface of the biomass participate in the reaction, and the increase in concentration nitrogen
308 promotes the removal of anions (Cao et al., 2014; Deng and Ting, 2005). The N spectrum (Figure

SD2) of MS is related to one component of N: pyrrolic-N (399.8 eV). However, after activation, the CMMS shows two peaks corresponding to pyrrolic-N (399.8 eV) and quaternary-N (402.0eV) (Matsoso et al., 2016).

The C spectra of MS and CMMS are de-convoluted into four different constituents of carbon at 284.8 corresponding to C–C/C=C, 286.4 related to C–O/C–N (alcohol/epoxy/alkoxy and N–sp^2–C (graphitic and pyrrolic) and N–sp^3–C (defected sp^3–C bonds), 287.98 for C=O (carboxyl)/N–C=O groups, and 289.0 corresponding to O–C=O (Figure SD3) (Khandelwal and Kumar, 2016). It was also found that apart from the increase in the intensity of oxygen at 532.9 (Spectrum not shown), no new components were detected after activation. This peak corresponds to oxygen in OH groups and its concentration increased from 27.7% to 28.3% after activation. The peak observed at 101.2 eV is attributed to Si^{2+}. The decrease of the concentration for this peak after biosorption indicated that Si might be involved in the reduction of Cr(VI) and complexation of Cr(III). Also, the MS and CMMS contained comparatively small quantities of S with narrow range spectra (~167eV) demonstrating the existence of oxygenated sulphur in the form of sulphonate groups.

3.6.1.2. Analysis for CMMS after biosorption

The oxidation state of the Cr bound to the CMMS was determined using XPS and the results are shown in Figure 4. The high-resolution spectra collected from (A) Cr onto fresh biomass; (B) Cr onto fresh biomass followed by loading with OII; (C) Cr onto fresh biomass in binary system; and (D) Cr onto OII-loaded biomass. For Cr_2O_3, major bands appeared at binding energies of 577.0–578.0eV, corresponding to $Cr2p_{3/2}$ orbital, and 586.0–588.0 eV matching $Cr2p_{1/2}$ orbital. On the other hand, the CrO_3 is characterized by higher binding energies; 581.0–582eV and 590.0–591.0eV, as the hexavalent form draws electrons more strongly than trivalent form.

From Figure 4, by relating the Cr peaks detected, it is possible to determine whether the bound Cr is in trivalent or hexavalent form. It can be confirmed that Cr(VI) was mostly reduced

335 to Cr(III) when brought into contact with the CMMS biosorbent, however, some Cr(VI) can still
336 be detected. This confirms that the removal mechanism of Cr(VI) by CMMS involves three steps
337 i) attraction of Cr(VI) ions to positively charged groups such as $–CN^{+}$; ii) reduction of Cr(VI) to
338 Cr(III) by neighbouring electron-donor groups such as –SiOH; iii) Cr(III) ions are bio-
339 sequestrated through metal ion coordination, ion exchange and chelating activities and then, part
340 of the reduced Cr(III) ions are freed into the aqueous solution because of electronic repulsion
341 (Albadarin et al., 2011b; Albadarin et al., 2014a). These conclusions are in good agreement with
342 the previously reported findings for the biosorption of Cr(VI) using seaweed (Murphy et al.,
343 2009). An estimation of the Cr(III)/Cr(VI) ratios in the different biosorption systems show that
344 the CMMS is more efficient to bio-reduce hexavalent chromium than other biosorbents i.e.
345 seaweed (Yang and Chen, 2008).

346 The elemental compositions of the Cr(VI)-loaded CMMS in the different biosorption
347 systems are summarised in Table 3. It is obvious that the CMMS had relatively large amounts of
348 Cr linked with their surface after reaction. The slight changes found in the atomic concentration
349 of carbon indicate that some CMMS leached during the experiment. The change in the
350 concentration of oxygen may be due to the biosorption of chromium hydroxides (Murphy et al.,
351 2009). The Cl element is coming from the activation reagent and the increase in the S an
352 indication of OII biosorption. From Table 3, the amount of loaded Cr before or after loading the
353 OII had comparable amounts of chromium bound to the CMMS surface (0.47 and 0.52%,
354 respectively) whereas a lower amount was bound to the CMMS in the binary system (0.27%)
355 and a maximum quantity was loaded in the Cr(VI) single system. These results agree with
356 previous sorption isotherm results presented in Table 2. Finally, the shifts in the peak at 400.0eV
357 indicate that hydrogen bonding/$\pi– \pi$ interactions and electrostatic attraction through –N=N– is
358 contributing in the removal mechanisms of OII dye.

359 3.6.2. FTIR and SEM analysis

360 FTIR spectroscopy was used in section 3.1. to identify the functionalities capable of
361 interacting with Cr(VI) and OII. The same technique is used in this section to determine the main
362 functionalities involved in the biosorption process. The spectra for the Cr(VI) and OII-loaded
363 CMMS in single and binary systems were recorded (data not shown here). The shifts and shape-
364 changes taking place in the –OH stretching band around 3430/cm indicates that the Orange II is
365 attached to the oxygen atoms on the CMMS forming monodentate, bidentate or tridentate bonds
366 and substituting the water molecules (Albadarin and Mangwandi, 2015; Benjamin and Leckie,
367 1981). The decrease in the intensity for the peak around 2100/cm indicate that –C≡N group was
368 involved in the biosorption process. Also the shifts of the peaks around 1600 to 1625/cm and
369 disappearance of the sulphonate group around 1329/cm after Cr(VI) and OII biosorption confirm
370 the involvement of the –C=O and $–SO_3$ in the process. New individual peaks at 1520 and 1600
371 1/cm due to benzene skeleton vibrations appear in the FTIR spectrum of OII-loaded CMMS.
372 Based on the analysis from the XPS, FTIR and the SEM, the removal of Cr(VI) and Orange II
373 from aqueous solutions can be illustrated as shown in Figure 5. It can be seen that electrostatic
374 attraction, hydrogen bonding and π– π interactions mechanisms are involved in the removal
375 process.

376 Finally, the Scanning electron micrographs showing the MS (A), CMMS (B), Cr-loaded
377 CMMS (C) and Orange II-loaded CMMS (D) morphology are presented in Figure 6. From the
378 images the fresh surfaces of the MS surface appear rough with a rugged morphology. After
379 chemical activation, the CMMS looks darker and more heterogeneous, making it a potential for
380 the biosorption of Orange II dye and Cr(VI) ions. The images present significant differences in
381 surface morphology between the MS and CMMS; these surface topographies variations are due
382 to the different quantities of available functionalities i.e. $–NH_2$ and –OH. After OII and Cr(VI)
383 biosorption, the morphology of the CMMS changed and the edges of the microstructure appear
384 to be less obvious than before the chromate ion biosorption. This confirms the loading of Orange

385 II and Cr(VI) onto the CMMS and indicate that ion exchange might be involved in the
386 biosorption process, especially after Cr(VI) reduction.

387 **4. CONCLUSIONS**

388 It can be concluded from the findings of this study that CMMS is capable of simultaneously
389 and consecutively removing both Cr(VI) and OII from synthetic wastewater by biosorption. The
390 CMMS biosorbents has preferential biosorption of OII over Cr(VI) in their aqueous mixtures at
391 acidic conditions, which is due to the fact that CMMC shows higher affinity to dye than to metal
392 ions. The performance of the CMMS on removal of OII was better, in consecutive and binary
393 systems. This suggests that the presences of Cr(IV) and OII ions in the systems does not result
394 in competition for biosorption sites but enhance the removal of the ions. It is hypothesised that
395 the improvement in the removal of OII biosorption is due to reduction in the electrostatic
396 repulsive forces between the large dye to presence of the chromium (III) ions. The above
397 conclusions and the high capacity for OII and Cr(VI) make this chemically modified by-product
398 biosorbent suitable for real wastewater treatment applications.

399 **5. REFERENCES**

400 Albadarin, A.B., Al-Muhtaseb, A.a.H., Al-laqtah, N.A., Walker, G.M., Allen, S.J., Ahmad, M.N.M., 2011a.
401 Biosorption of toxic chromium from aqueous phase by lignin: mechanism, effect of other metal ions and salts.
402 Chemical Engineering Journal 169, 20-30.
403 Albadarin, A.B., Al-Muhtaseb, A.a.H., Walker, G.M., Allen, S.J., Ahmad, M.N.M., 2011b. Retention of toxic
404 chromium from aqueous phase by H3PO4-activated lignin: Effect of salts and desorption studies. Desalination 274,
405 64-73.
406 Albadarin, A.B., Glocheux, Y., Ahmad, M.N.M., Walker, G.M., Mangwandi, C., 2014a. Novel comparison of
407 kinetic models for the adsorption-coupled reduction of Cr(VI) using untreated date pit biomaterial. Ecological
408 Engineering 70, 200-205.
409 Albadarin, A.B., Mangwandi, C., 2015. Mechanisms of Alizarin Red S and Methylene blue biosorption onto olive
410 stone by-product: Isotherm study in single and binary systems. Journal of Environmental Management 164, 86-93.
411 Albadarin, A.B., Mangwandi, C., Al-Muhtaseb, A.a.H., Walker, G.M., Allen, S.J., Ahmad, M.N.M., 2012. Kinetic
412 and thermodynamics of chromium ions adsorption onto low-cost dolomite adsorbent. Chemical Engineering Journal
413 179, 193-202.
414 Albadarin, A.B., Mangwandi, C., Walker, G.M., Allen, S.J., Ahmad, M.N.M., Khraisheh, M., 2013. Influence of
415 solution chemistry on Cr(VI) reduction and complexation onto date-pits/tea-waste biomaterials. Journal of
416 Environmental Management 114, 190-201.
417 Albadarin, A.B., Mo, J., Glocheux, Y., Allen, S., Walker, G., Mangwandi, C., 2014b. Preliminary investigation of
418 mixed adsorbents for the removal of copper and methylene blue from aqueous solutions. Chemical Engineering
419 Journal 255, 525-534.
420 Anandkumar, J., Mandal, B., 2011. Adsorption of chromium(VI) and Rhodamine B by surface modified tannery
421 waste: Kinetic, mechanistic and thermodynamic studies. Journal of Hazardous Materials 186, 1088-1096.
422 Babel, S., Kurniawan, T.A., 2004. Cr(VI) removal from synthetic wastewater using coconut shell charcoal and
423 commercial activated carbon modified with oxidizing agents and/or chitosan. Chemosphere 54, 951-967.

Benjamin, M.M., Leckie, J.O., 1981. Multiple-site adsorption of Cd, Cu, Zn, and Pb on amorphous iron oxyhydroxide. Journal of Colloid and Interface Science 79, 209-221.
Bouberka, Z., Khenifi, A., Benderdouche, N., Derriche, Z., 2006. Removal of Supranol Yellow 4GL by adsorption onto Cr-intercalated montmorillonite. Journal of Hazardous Materials 133, 154-161.
Cao, J.-S., Lin, J.-X., Fang, F., Zhang, M.-T., Hu, Z.-R., 2014. A new absorbent by modifying walnut shell for the removal of anionic dye: Kinetic and thermodynamic studies. Bioresource Technology 163, 199-205.
Correia, V.M., Stephenson, T., Judd, S.J., 1994. Characterisation of textile wastewaters - a review. Environmental Technology 15, 917-929.
Daneshvar, E., Kousha, M., Koutahzadeh, N., Sohrabi, M.S., Bhatnagar, A., 2013. Biosorption and bioaccumulation studies of acid Orange 7 dye by Ceratophylum demersum. Environmental Progress & Sustainable Energy 32, 285-293.
Deng, S., Bai, Chen, J.P., 2003. Aminated Polyacrylonitrile Fibers for Lead and Copper Removal. Langmuir 19, 5058-5064.
Deng, S., Ting, Y.P., 2005. Polyethylenimine-Modified Fungal Biomass as a High-Capacity Biosorbent for Cr(VI) Anions: Sorption Capacity and Uptake Mechanisms. Environmental Science & Technology 39, 8490-8496.
Fanun, M., 2014. The role of colloidal systems in environmental protection. Elsevier, 720 pages.
Ferhat, M., Kadouche, S., Drouiche, N., Messaoudi, K., Messaoudi, B., Lounici, H., 2016. Competitive adsorption of toxic metals on bentonite and use of chitosan as flocculent coagulant to speed up the settling of generated clay suspensions. Chemosphere 165, 87-93.
Freundlich, H.M.F., 1906. Over the adsorption in solution. Journal of Physical Chemistry 57, 385-471.
Gómez, J.M., Galán, J., Rodríguez, A., Walker, G.M., 2014. Dye adsorption onto mesoporous materials: PH influence, kinetics and equilibrium in buffered and saline media. Journal of Environmental Management 146, 355-361.
Heibati, B., Rodriguez-Couto, S., Turan, N.G., Ozgonenel, O., Albadarin, A.B., Asif, M., Tyagi, I., Agarwal, S., Gupta, V.K., 2015. Removal of noxious dye—Acid Orange 7 from aqueous solution using natural pumice and Fe-coated pumice stone. Journal of Industrial and Engineering Chemistry 31, 124-131.
Ho, Y.S., McKay, G., 1999. Pseudo-second order model for sorption process. Process Biochemistry 34, 451–465.
Karthik, C., Ramkumar, V.S., Pugazhendhi, A., Gopalakrishnan, K., Arulselvi, P.I., 2017. Biosorption and biotransformation of Cr(VI) by novel Cellulosimicrobium funkei strain AR6. Journal of the Taiwan Institute of Chemical Engineers 70, 282-290.
Khandelwal, M., Kumar, A., 2016. One-pot environmentally friendly amino acid mediated synthesis of N-doped graphene-silver nanocomposites with an enhanced multifunctional behavior. Dalton Transactions 45, 5180-5195.
Kurniawan, T.A., Chan, G.Y.S., Lo, W.-h., Babel, S., 2006. Comparisons of low-cost adsorbents for treating wastewaters laden with heavy metals. Science of The Total Environment 366, 409-426.
Kyzas, G.Z., Lazaridis, N.K., Kostoglou, M., 2013. On the simultaneous adsorption of a reactive dye and hexavalent chromium from aqueous solutions onto grafted chitosan. Journal of Colloid and Interface Science 407, 432-441.
Lagergren, S., 1898. Zur theorie der sogenannten adsorption gelöster stoffe KungligaSvenska Vetenskapsakademiens, Handlingar 24, 1–39.
Langmuir, I., 1916. The constitution and fundamental properties of solids and liquids,. Journal of the American Chemical Society 38, 2221-2295.
Li, K., Li, P., Cai, J., Xiao, S., Yang, H., Li, A., 2016. Efficient adsorption of both methyl orange and chromium from their aqueous mixtures using a quaternary ammonium salt modified chitosan magnetic composite adsorbent. Chemosphere 154, 310-318.
Li, L.-L., Feng, X.-Q., Han, R.-P., Zang, S.-Q., Yang, G., 2017. Cr(VI) removal via anion exchange on a silver-triazolate MOF. Journal of Hazardous Materials 321, 622-628.
Liu, Z., Zhang, F., Liu, T., Peng, N., Gai, C., 2016. Removal of azo dye by a highly graphitized and heteroatom doped carbon derived from fish waste: Adsorption equilibrium and kinetics. Journal of Environmental Management 182, 446-454.
Matsoso, B.J., Ranganathan, K., Mutuma, B.K., Lerotholi, T., Jones, G., Coville, N.J., 2016. Time-dependent evolution of the nitrogen configurations in N-doped graphene films. RSC Advances 6, 106914-106920.
Mishra, A., Tripathi, B.D., Rai, A.K., 2016. Packed-bed column biosorption of chromium(VI) and nickel(II) onto Fenton modified Hydrilla verticillata dried biomass. Ecotoxicology and Environmental Safety 132, 420-428.
Mungasavalli, D.P., Viraraghavan, T., Jin, Y.-C., 2007. Biosorption of chromium from aqueous solutions by pretreated Aspergillus niger: Batch and column studies. Colloids and Surfaces A: Physicochemical and Engineering Aspects 301, 214-223.
Murphy, V., Tofail, S.A.M., Hughes, H., McLoughlin, P., 2009. A novel study of hexavalent chromium detoxification by selected seaweed species using SEM-EDX and XPS analysis. Chemical Engineering Journal 148, 425-433.
Naushad, M., Ahamad, T., Sharma, G., Al-Muhtaseb, A.a.H., Albadarin, A.B., Alam, M.M., Alothman, Z.A., Alshehri, S.M., Ghfar, A.A., 2016. Synthesis and characterization of a new starch/SnO2 nanocomposite for efficient adsorption of toxic Hg2+ metal ion. Chemical Engineering Journal 300, 306-316.

Park, D., Lim, S.-R., Yun, Y.-S., Park, J.M., 2007. Reliable evidences that the removal mechanism of hexavalent chromium by natural biomaterials is adsorption-coupled reduction. Chemosphere 70, 298-305.
Redlich, O., Peterson, D.L., 1959. A useful adsorption isotherm. Journal of Physical Chemistry 63, 1024-1026.
Salameh, Y., Albadarin, A.B., Allen, S., Walker, G., Ahmad, M.N.M., 2015. Arsenic(III,V) adsorption onto charred dolomite: Charring optimization and batch studies. Chemical Engineering Journal 259, 663-671.
Salvi, N.A., Chattopadhyay, S., 2016. Biosorption of Azo dyes by spent Rhizopus arrhizus biomass. Applied Water Science, 1-14.
Šillerová, H., Chrastný, V., Čadková, E., Komárek, M., 2014. Isotope fractionation and spectroscopic analysis as an evidence of Cr(VI) reduction during biosorption. Chemosphere 95, 402-407.
Song, W., Shi, T., Yang, D., Ye, J., Zhou, Y., Feng, Y., 2015. Pretreatment effects on the sorption of Cr(VI) onto surfactant-modified zeolite: Mechanism analysis. Journal of Environmental Management 162, 96-101.
Volesky, B., 2007. Biosorption and me. Water Research 41, 4017-4029.
Wu, Y., Hu, Y., Xie, Z., Feng, S., Li, B., Mi, X., 2011. Characterization of Biosorption Process of Acid Orange 7 on Waste Brewery's Yeast. Applied Biochemistry and Biotechnology 163, 882-894.
Yang, L., Chen, J.P., 2008. Biosorption of hexavalent chromium onto raw and chemically modified Sargassum sp. Bioresource Technology 99, 297-307.
Zhu, T., Huang, W., Zhang, L., Gao, J., Zhang, W., 2017. Adsorption of Cr(VI) on cerium immobilized cross-linked chitosan composite in single system and coexisted with Orange II in binary system. International Journal of Biological Macromolecules 103, 605-612.

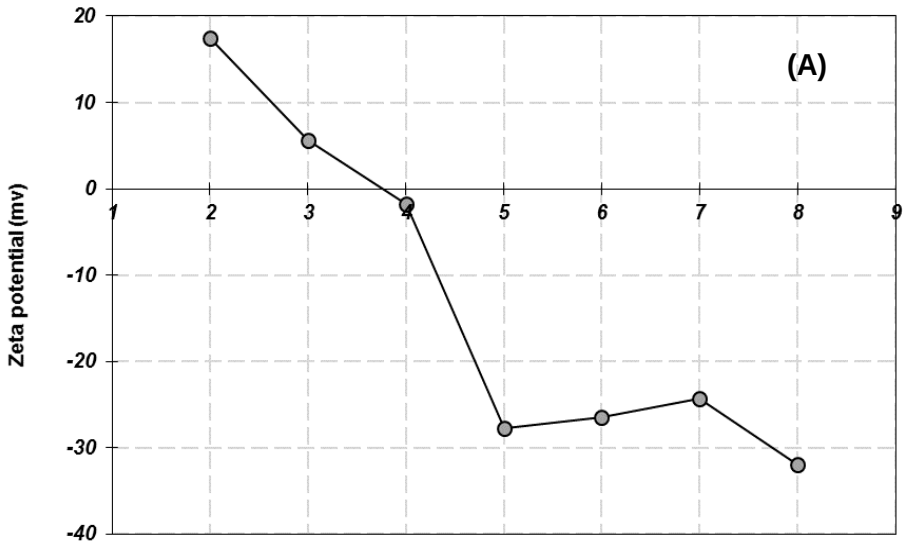

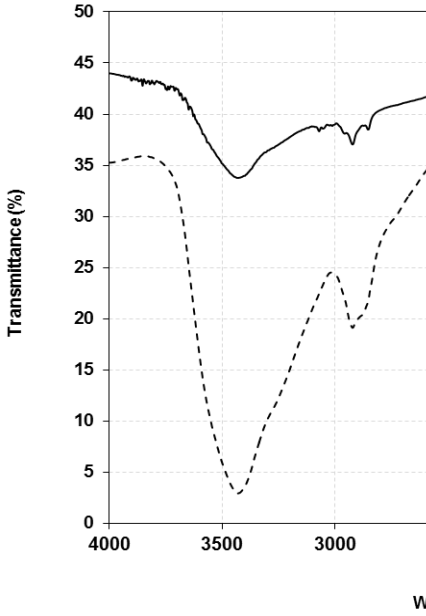

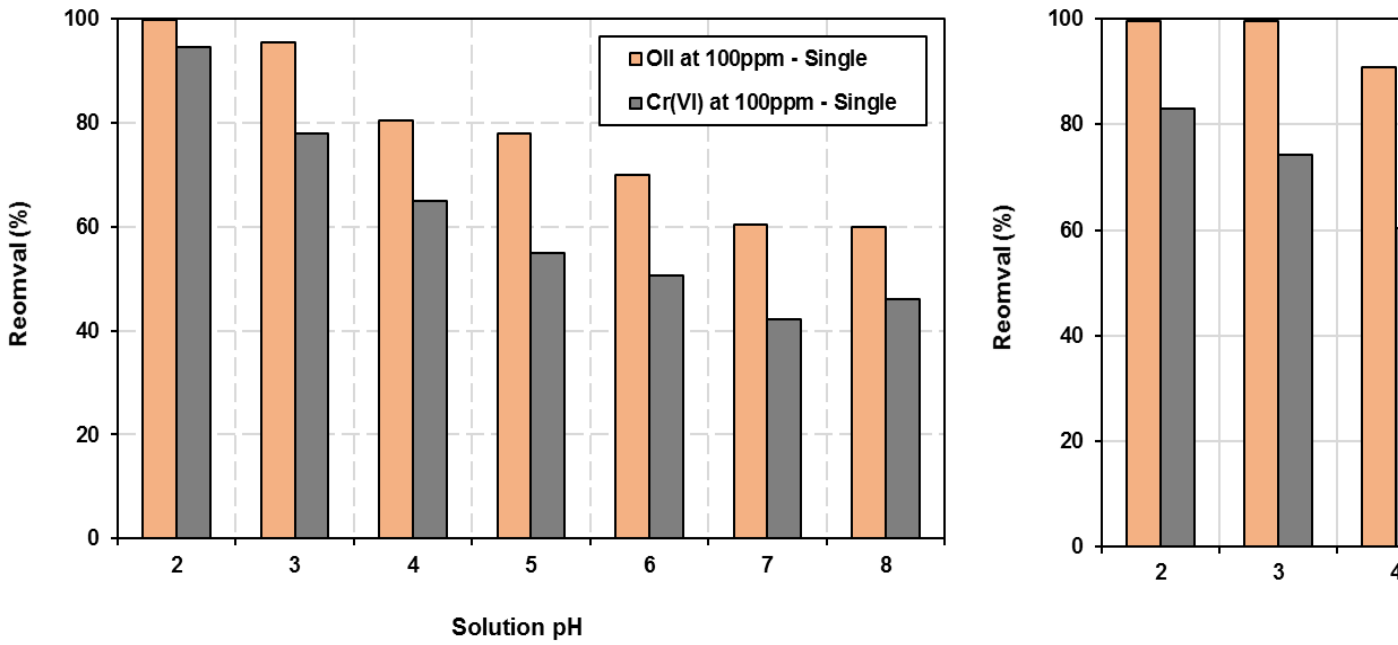

515

516 Figure 1: Zeta potential (A) and FTIR (B) analyses of CMMS biosorbent and the effect of pH

517 on the biosorption of Orange II dye and Cr(VI) in single (left) and binary (right) systems.

518

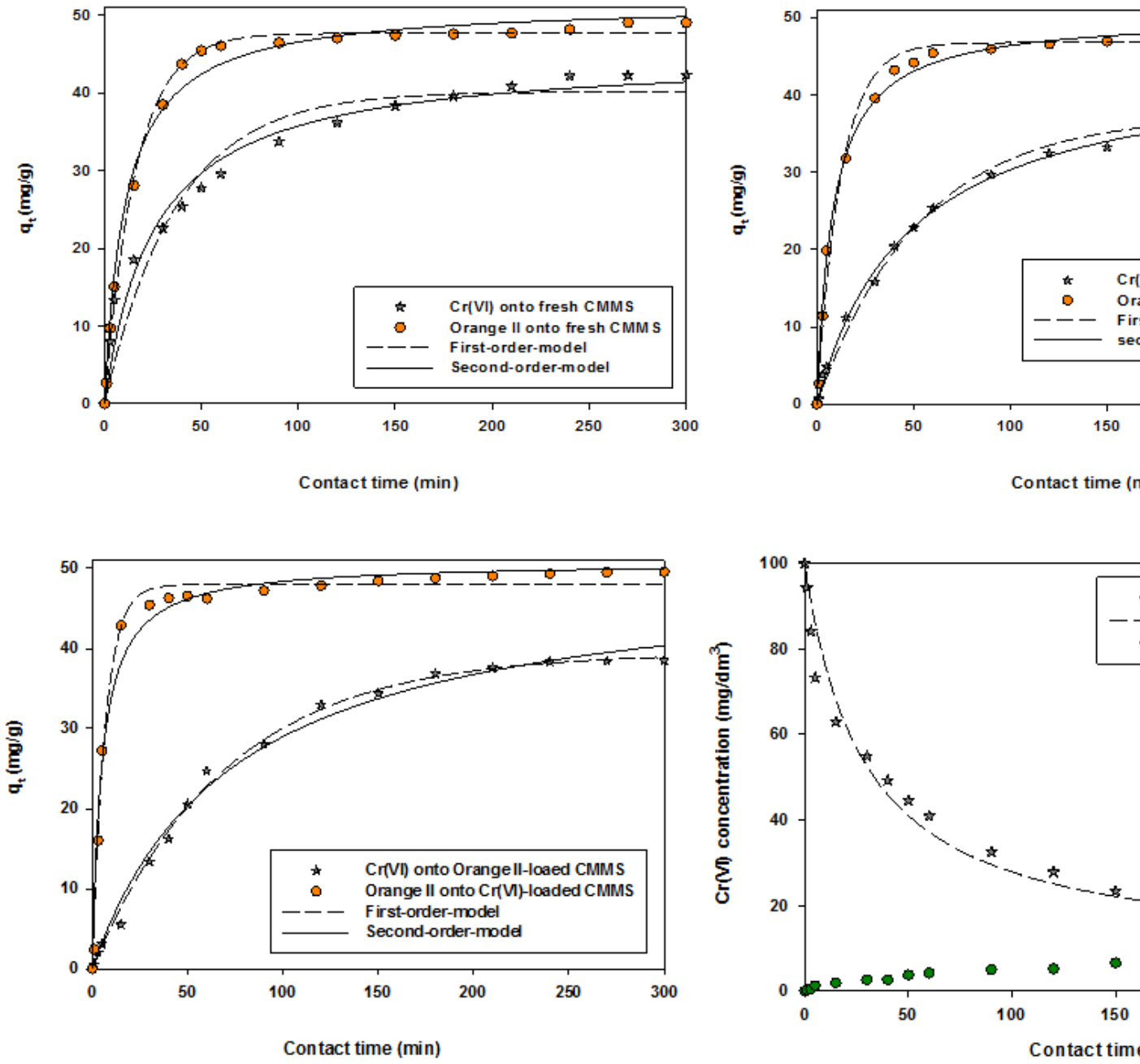

519
520 Figure 2: The fittings for the pseudo first, second order and redox models for the
521 biosorption of OII dye and Cr(VI) onto CMMS.

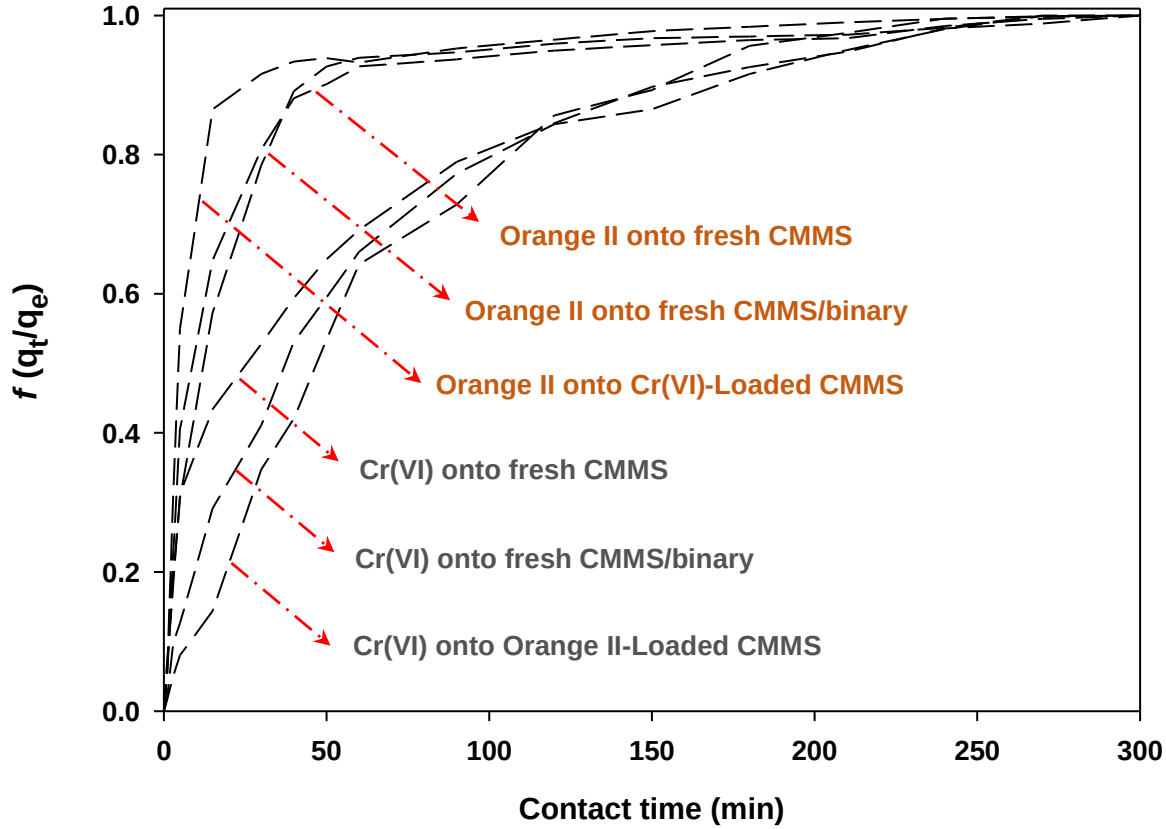

Figure 3: The OII and Cr (VI) fractional uptakes, *f*, vs time in different systems.

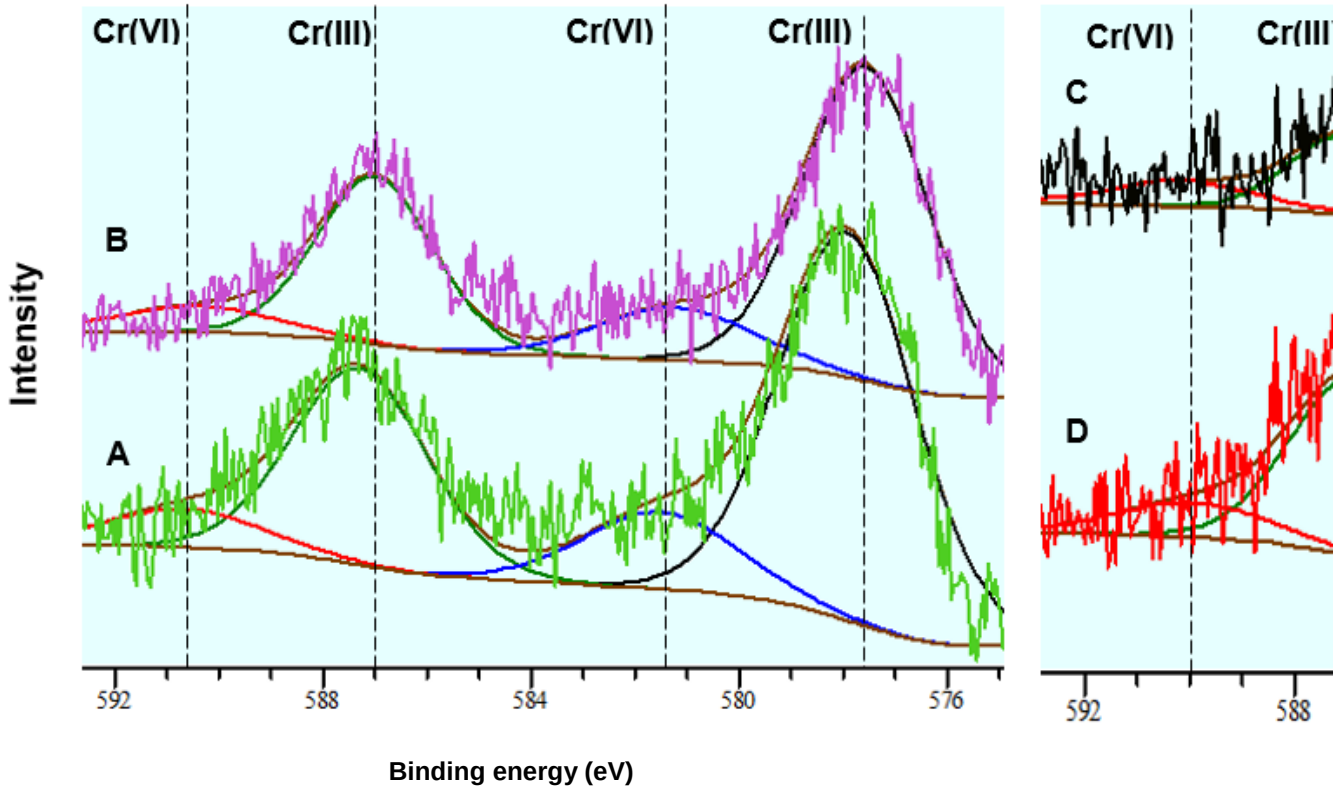

528

529 Figure 4: High resolution Cr2p spectra for CMMS biosorbent.

530

531

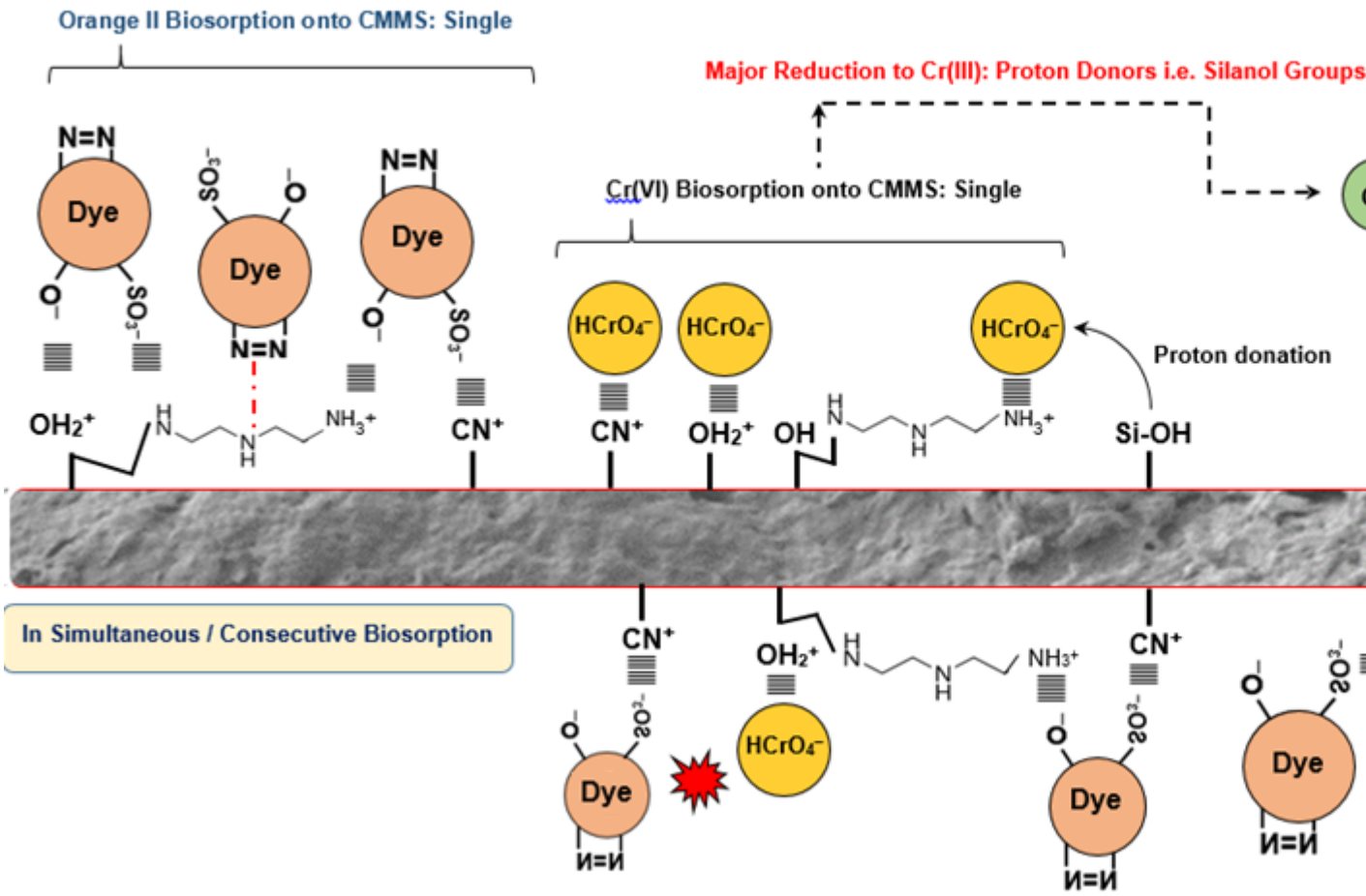

532

533 Figure 5: Schematic diagram illustrating the mechanisms of OII and Cr(VI) removal by

534 CMMS biosorbent in different systems.

535

536

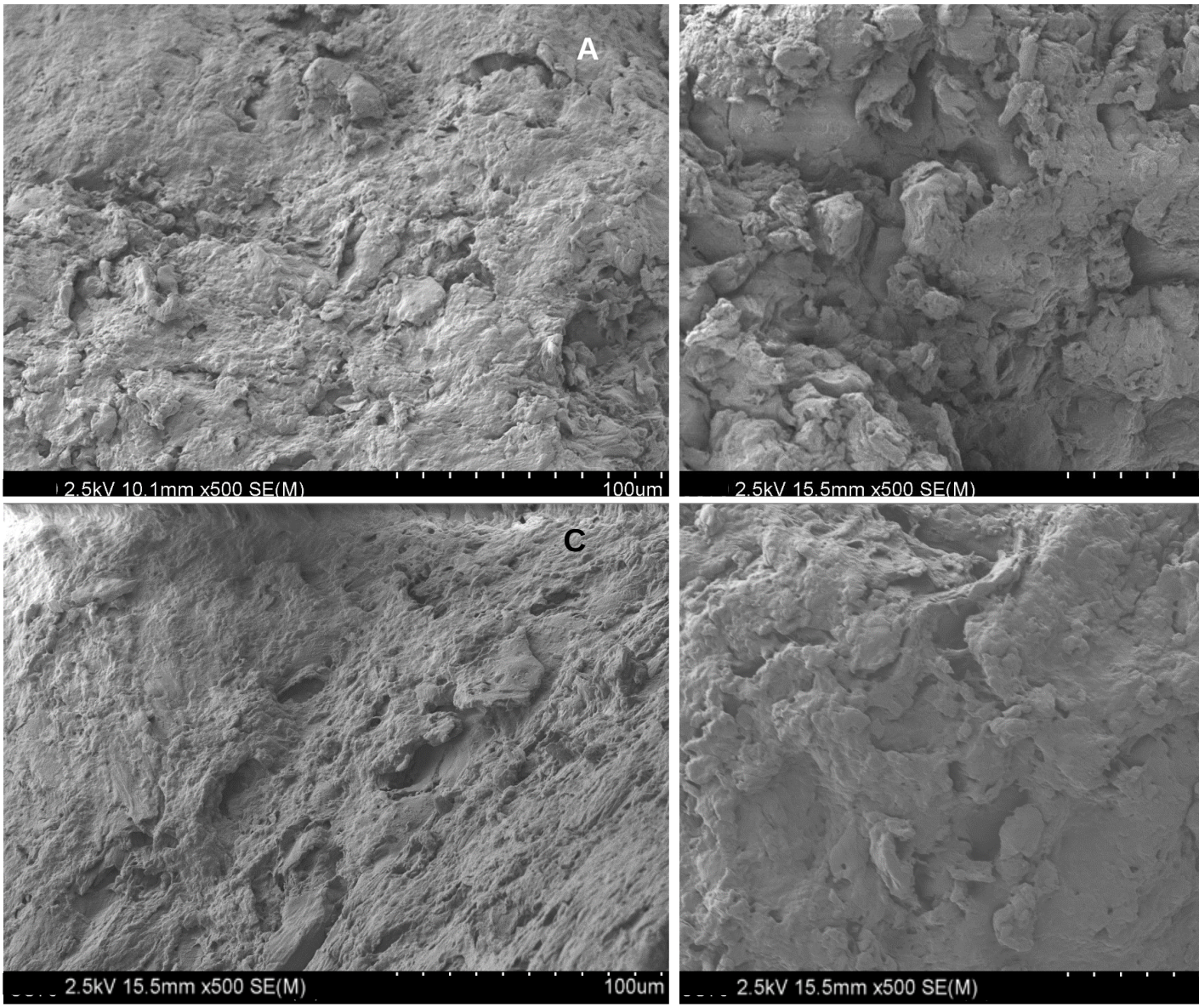

537

538 Figure 6: Scanning electron micrographs showing the MS (A), CMMS (B), Cr-loaded

539 CMMS (C) and OII-loaded CMMS (D) surface morphologies.

540

541

542 **1 Supplementary Data**

543

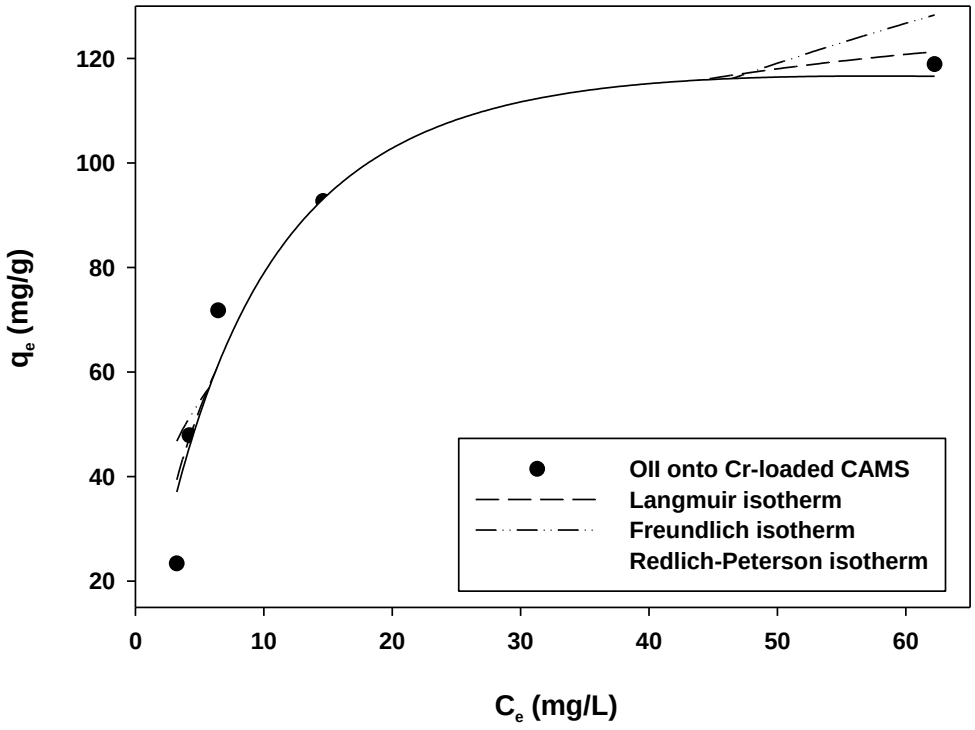
120
100
80
60
40
20
0
10
20
30
40
50
60
q_e (mg/g)
C_e (mg/L)
OII onto Cr-loaded CAMS
Langmuir isotherm
Freundlich isotherm
Redlich-Peterson isotherm

544

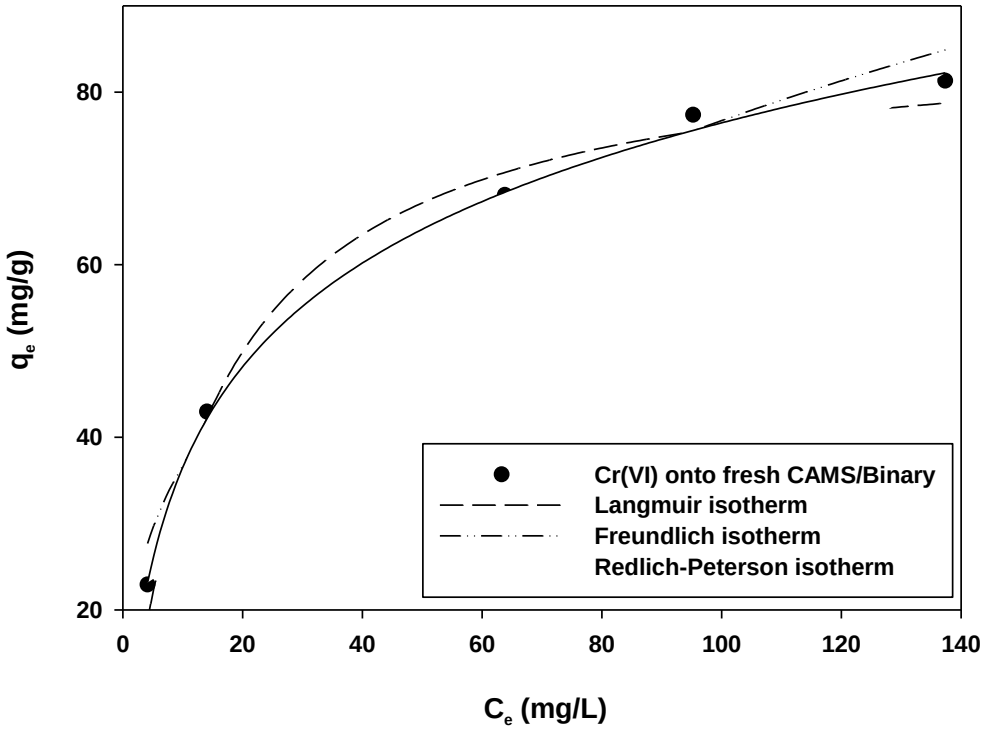
80
60
40
20
0
20
40
60
80
100
120
140
q_e (mg/g)
C_e (mg/L)
Cr(VI) onto fresh CAMS/Binary
Langmuir isotherm
Freundlich isotherm
Redlich-Peterson isotherm

545

546 SD1: Isotherm fittings for the biosorption of OII onto Cr(VI)-loaded CMMS and Cr(VI) biosorption onto unloaded CMMS.

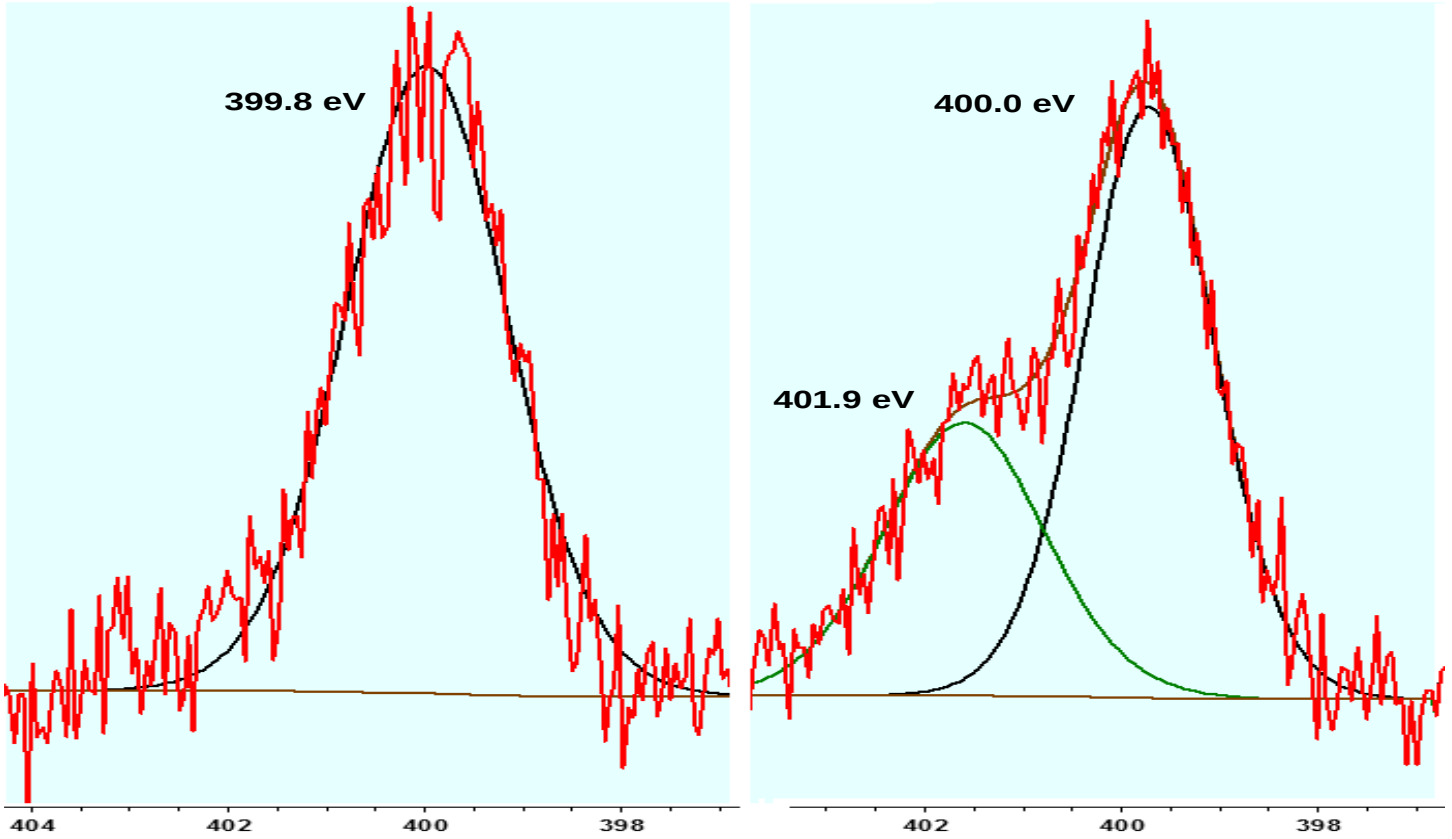

547

548 SD2 : The XPS spectrum for N in MS and CMMS.

549

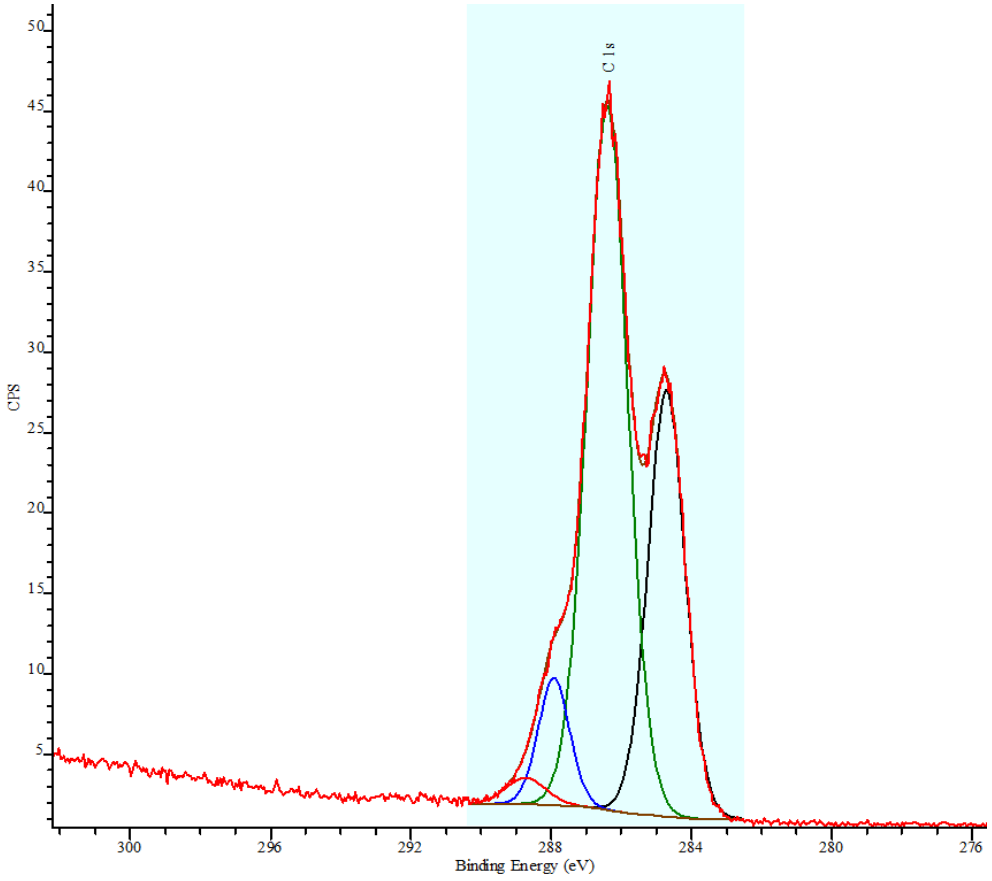

550

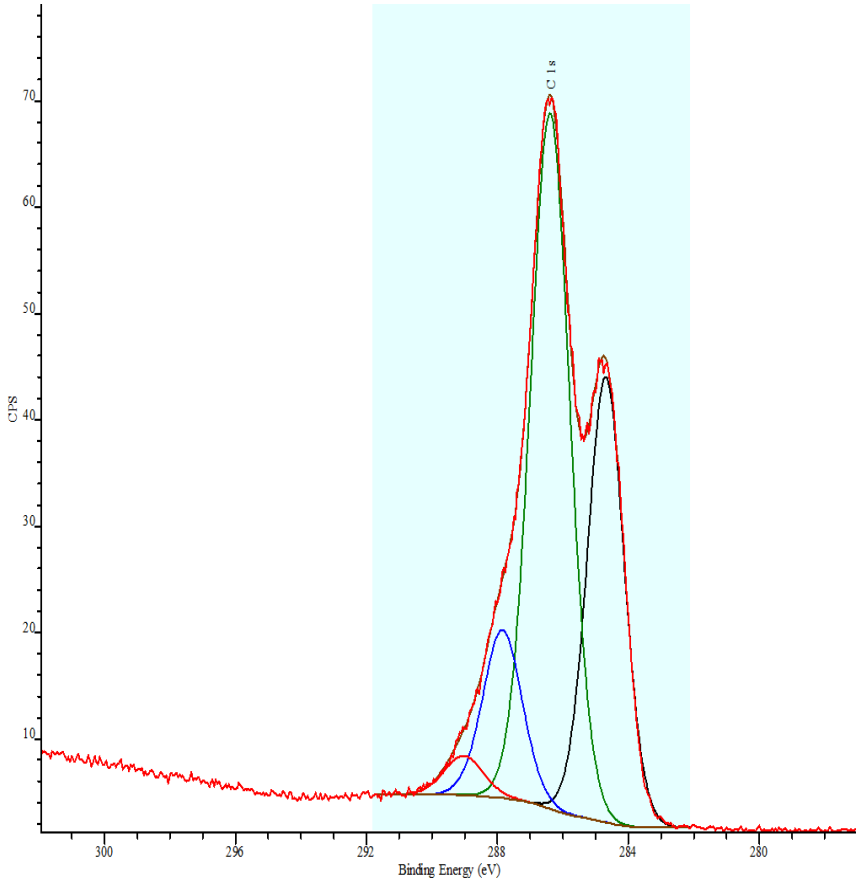

551

552 SD3: Carbon spectrum for raw Masau Stone (MS) and chemically activated Masau Stone (CMMS).

Table 1: Kinetic constants determined for the biosorption of OII and Cr(VI) onto CMMS in different systems.

System	Pseudo first order				Pseudo second order			External mass transfer*
	q_{exp}	q_e	k_1	R^2	q_e	k_2	R^2	k_s
Cr(VI) only	43.44	40.11	0.027	0.980	44.93	9.0×10^4	0.995	0.061
Cr(VI)/binary	38.44	37.33	0.019	0.994	44.85	5.0×10^4	0.993	0.038
Cr(VI) onto Orange II-CMMS	38.52	39.43	0.014	0.997	40.20	3.0×10^4	0.993	0.018
Orange II only	49.01	47.63	0.062	0.997	51.55	1.8×10^3	0.993	0.095
Orange II/binary	49.18	47.76	0.080	0.988	50.30	2.4×10^3	0.994	0.111
Orange II onto Cr(VI)-CMMS	49.56	47.96	0.145	0.990	50.79	3.9×10^3	0.982	0.153

	Redox model		
	k_{redox}	C_{OC}	R^2
Cr(VI) only	4.0×10^4	44.03	0.984
Cr(VI)/binary	2.0×10^4	41.80	0.998
Cr(VI) onto Orange II-CMMS	1.0×10^4	40.44	0.992

*Rate constant of external mass transfer determined from the plots of C_t/C_o against time.

563 Table 2: Isotherm constants for the biosorption processes of OII and Cr(VI) onto CMMS at different systems.

System	Langmuir isotherm			Freundlich isotherm			Redlich-Peterson isotherm			
	q_{max}	b	R^2	K_F	$1/n$	R^2	K_R	a_R	β	R^2
Cr(VI) only	87.32	0.066	0.978	17.57	0.320	0.988	11.21	0.314	0.819	0.997
Cr(VI)/binary	66.99	0.082	0.923	18.45	0.249	0.847	5.208	0.069	0.998	0.923
Cr(VI) onto OII-CMMS	81.26	0.048	0.974	15.80	0.336	0.883	3.407	0.015	0.987	0.985
OII only	116.5	0.111	0.995	26.82	0.325	0.943	14.32	0.149	0.955	0.995
OII/binary	129.2	0.165	0.967	32.47	0.335	0.925	24.26	0.239	0.938	0.969
OII onto Cr(VI)-CMMS	136.8	0.125	0.942	31.39	0.341	0.845	13.75	0.049	0.997	0.952

564

565

566

567

568

569

570

571

572

573 Table 3: Elemental composition of unloaded and OII and Cr(VI)-loaded CMMS as

574 determined using XPS.

Elements	**MS**	**CMMS**	**Cr onto CMMS**	**Cr onto CMMS followed by loading with OII**	**Cr onto CMMS in binary system**	**Cr onto OII-loaded CMMS**
O 1s	27.70%	28.30%	30.55%	33.01%	32.22%	30.66%
C 1s	68.90%	67.32%	64.54%	62.13%	63.28%	65.89%
N 1s	2.10%	3.20%	3.26%	3.25%	3.17%	2.00%
Cl 2p	–	0.20%	0.25%	0.12%	0.25%	0.23%
S 2p	0.30%	0.28%	0.26%	0.37%	0.32%	0.34%
Si 2p	1.10%	0.70%	0.44%	0.65%	0.49%	0.06%
Cr 2p	–	–	0.70%	0.47%	0.27%	0.52%
Cr(VI)/Cr(III)	–	–	23.07%	23.68%	32.42%	21.73%

575

576